Inorganic Chemistry
Article
Cite This: Inorg. Chem. XXXX, XXX, XXX−XXX
pubs.acs.org/IC

Oximato-Based Ligands in 3*d*/4*f*-Metal Cluster Chemistry: A Family of {Cu_3Ln} Complexes with a "Propeller"-like Topology and Single-Molecule Magnetic Behavior

Anne Worrell,[†] Di Sun,[‡] Julia Mayans,[§] Christos Lampropoulos,[∥] Albert Escuer,[§] and Theocharis C. Stamatatos*[,†]

[†]Department of Chemistry, 1812 Sir Isaac Brock Way, Brock University, L2S 3A1 St. Catharines, Ontario, Canada

[‡]Key Lab of Colloid and Interface Chemistry, Ministry of Education, School of Chemistry and Chemical Engineering, Shandong University, Jinan 250100, P. R. China

[§]Departament de Quimica Inorgànica i Orgànica and Institut de Nanociencia i Nanotecnologia (IN^{2}UB), Universitat de Barcelona, Martí i Franqués 1-11, 08028 Barcelona, Spain

[∥]Department of Chemistry, University of North Florida, 1 UNF Drive, Jacksonville, Florida 32224, United States

Supporting Information

ABSTRACT: The organic chelating and bridging ligands 9,10-phenanthrenedione-9-oxime (phenoxH) and 9,10-phenanthrenedione-9,10-dioxime ($phendoxH_2$) were synthesized and subsequently employed for the first time in heterometallic 3*d*/4*f*-metal cluster chemistry. The general reaction between $CuCl_2{\cdot}2H_2O$, $LnCl_3{\cdot}6H_2O$, phenoxH, and NEt_3 in a 1:2:2:4 molar ratio, in a solvent mixture comprising MeCN and MeOH, afforded brown crystals of a new family of $[Cu_3LnCl_3(phenox)_6(MeOH)_3]$ clusters (Ln = Gd (**1**), Tb (**2**), Dy (**3**)) that possess an unprecedented $[Cu_3Ln(\mu\text{-}NO)_6]^{3+}$ "propeller"-like core. Complexes **1**−**3** are the first {Cu_3Ln} clusters in which the outer Cu^{II} and the central Ln^{III} atoms are solely bridged by diatomic oximato bridges. The {Cu-N-O-Ln} bridging units are very distorted with torsion angles spanning the range 35.5−48.9° and 25.2−55.6° in **1** and **2**, respectively. As a result, complexes **1**−**3** are antiferromagnetically coupled, in agreement with previously reported magneto-structural criteria for oximato-bridged Cu/Ln complexes. The magnetic susceptibility data for all complexes were nicely fit to an isotropic spin Hamiltonian (for **1**) or a Hamiltonian that accounts for the spin of the Cu^{II} atoms, the spin component of the Ln^{III}, the spin−orbit coupling (λ), an axial ligand-field component around the Ln^{III} atoms (Δ), and the Zeeman effect (for the anisotropic **2** and **3**). The resulting fit parameters were $J = -1.34$ cm^{-1} and $g = 2.10$ (**1**), $J = -1.42$ cm^{-1}, $g_{Cu} = 2.10$, and $\Delta = -26.3$ cm^{-1} (**2**), and $J = -1.70$ cm^{-1}, $g_{Cu} = 2.05$, and $\Delta = -38.1$ cm^{-1} (**3**). The reported fitting procedure, implemented in the PHI program, is here used for the first time. Even if this method is only valid in high-symmetry Ln environments, when it is properly used allows a very simple and efficient method to obtain the exchange parameters. In light of the negative anisotropy, compounds **2** and **3** were found to exhibit frequency-dependent tails of out-of-phase signals in the presence of a small external *dc* field, characteristic of the slow magnetization relaxation of a single-molecule magnet. By using the Kramers−Kronig equations, the effective energy barriers (U_{eff}) were derived and reported as $U_{eff} = 10.1$ and 5.4 cm^{-1} for **2** and **3**, respectively.

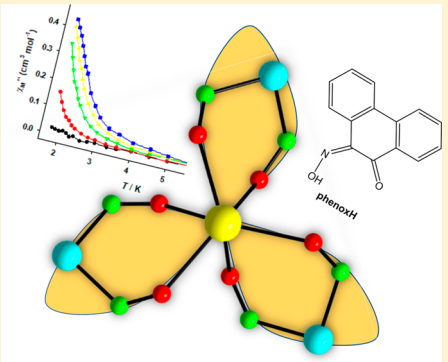

INTRODUCTION

The interest in polynuclear Cu^{II}/Ln^{III} metal complexes (coordination clusters or simply metal clusters) mainly stems from the combined ability of these metal ions to stabilize high-nuclearity structures with architecturally beautiful topologies and occasionally fascinating magnetic properties.[1] Ferromagnetic exchange interactions are frequently observed in many Cu^{II}/Gd^{III} complexes owing to the orthogonality of the *d*- and *f*-orbitals and consequently the efficient electron transfer from the singly occupied 3*d* Cu^{II} orbital to an empty 5*d* Gd^{III} orbital.[1,2] The $Cu^{II}\cdots Ln^{III}$ (Ln = Tb or Dy) interactions can also be ferromagnetic, but these are more rarely observed due to the concurrent presence of first-order angular momentum.[3] Other factors are also reported to affect the sign and magnitude of the $Cu^{II}\cdots Ln^{III}$ magnetic exchange interactions, such as the type of the bridging ligand(s), the degree of planarity of the bridging core, and the hinge angle.[3]

In isotropic Cu^{II}/Gd^{III} compounds, weak and ferromagnetic exchange interactions can lead to large spin ground states and subsequently to an appreciable magnetocaloric effect (MCE), i.e., the magnetic material's thermal response upon exposure to a magnetic field change.[4] These compounds can thus act as molecular magnetic refrigerants.[5] In contrast, the presence of

Received: September 2, 2018

DOI: 10.1021/acs.inorgchem.8b02495
Inorg. Chem. XXXX, XXX, XXX−XXX

significant magnetic anisotropy, as reflected in a large and negative zero-field splitting parameter, D, renders some of these Cu^{II}/Ln^{III} (Ln = Tb and Dy) analogues suitable candidates for the observation of single-molecule magnetic properties. Single-molecule magnets (SMMs) are molecular species that retain their magnetization in the absence of an applied field.[6] Experimentally, SMMs show superparamagnet-like properties and exhibit slow relaxation of their magnetization that is usually detected from the appearance of frequency-dependent out-of-phase alternating-current (ac) signals.

For the synthesis of new Cu^{II}/Ln^{III} clusters, the choice of the primary bridging/chelating organic ligand remains one of the most appealing challenges. From an extensive literature survey, it becomes apparent that alkoxido-based organic chelates have dominated the field and contributed the most to the synthesis of Cu^{II}/Ln^{III} clusters with interesting structural and magnetic properties.[7] Our group has had a longstanding interest in the synthesis and use of new mono- and dioximato chelates as a means of isolating heterometallic complexes with unprecedented topologies and nontrivial physicochemical properties (i.e., magnetic, optical, and catalytical).[8] To this end, we recently reported a series of new Cu^{II}/Ln^{III} clusters of different nuclearities (i.e., $\{Cu_6Ln_{12}\}$[9] and $\{Cu_6Ln_2\}$[10]) and topologies from the use of 2,6-diacetylpyridine dioxime ($dapdoH_2$) and acenaphthenequinone dioxime ($acndH_2$), respectively (Scheme 1).

Scheme 1. Structural Formulae and Abbreviations of the Organic Chelating/Bridging Ligands Discussed in the Text

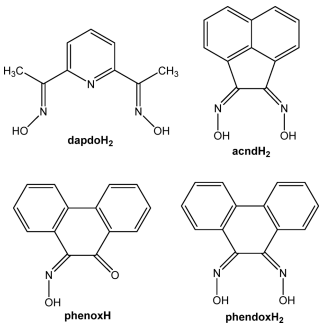

The $acndH_2$ ligand inspired us to move this research forward and synthesize the structurally similar mono- and dioxime ligands, 9,10-phenanthrenedione-9-oxime (phenoxH) and 9,10-phenanthrenedione-9,10-dioxime ($phendoxH_2$, Scheme 1). This first step has been successful, and therefore, we decided to systematically explore the coordination capabilities of phenoxH and $phendoxH_2$ in Cu^{II}/Ln^{III} chemistry. Herein, we report the synthesis, structures, and detailed magnetic characterization of a new family of $[Cu_3LnCl_3(phenox)_6(MeOH)_3]$ complexes (Ln = Gd (**1**), Tb (**2**), Dy (**3**)) bearing an unprecedented $[Cu_3Ln(\mu\text{-}NO)_6]^{3+}$ "propeller"-like core and exhibiting some interesting magnetic properties.

EXPERIMENTAL SECTION

Synthesis and Physical Measurements. All manipulations were performed under aerobic conditions using materials (reagent grade) and solvents as received unless otherwise noted. The organic ligands phenoxH and $phendoxH_2$ were prepared and characterized according to modified literature methods described elsewhere.[11,12] Infrared spectra were recorded in the solid state on a Bruker's FT-IR spectrometer (ALPHA's Platinum ATR single reflection) in the 4000−400 cm^{-1} range. Elemental analyses (C, H, and N) were performed on a PerkinElmer 2400 Series II Analyzer. Electrospray ionization (ESI) mass spectra (MS) were taken on a Bruker HCT Ultra mass spectrometer from MeOH solutions of both organic ligands. NMR spectra were obtained on a Bruker Avance DPX-400 MHz instrument and are referenced to the residual proton signal of the deuterated solvent for ^1H spectra according to published values. Magnetic susceptibility measurements were carried out on polycrystalline samples of **1**−**3** with an MPMS5 Quantum Design susceptometer operating in the temperature range 30−300 K under a magnetic field of 0.3 T and a small field of 0.03 T in the 30−2 K region to avoid saturation effects at low temperatures. Direct current (dc) magnetic susceptibility data were fit with the program PHI.[13] The quality of the fits was parametrized as the $R = (\chi_M T_{exp} - \chi_M T_{calc})^2/(\chi_M T_{exp})^2$ factor. Pascal's constants were used to estimate the diamagnetic correction,[14] which was subtracted from the experimental susceptibility to give the molar paramagnetic susceptibility (χ_M) for each complex.

Synthesis of phenoxH. To an orange suspension of 9,10-phenanthrenedione (2.08 g, 10.0 mmol) in EtOH (50 mL) was added a solution of $NH_2OH{\cdot}HCl$ (0.65 g, 10.0 mmol) and pyridine (0.81 mL, 10.0 mmol) in the same solvent (20 mL). The resulting suspension was refluxed for 30 min, during which time the solids dissolved and the solution turned to clear orange. The resulting solution was cooled, filtered, and left for slow evaporation at room temperature. The next day, an orange microcrystalline solid of the titled mono-oxime was formed, which was collected by fitration, washed with cold EtOH (2 × 5 mL), and dried under vacuum for 24 h. The yield was 96%. M.p.: 156−159 °C. ^1H NMR ($CDCl_3$, 400 MHz) δ (ppm): 7.48−7.58 (s, 3H), 7.80−7.84 (m, 1H), 8.13 (d, J = 7.8 Hz, 1H), 8.21 (d, J = 8.1 Hz, 1H), 8.37−8.45 (m, 2H), 12.15 (m, 1H). Elemental analysis (%) calcd for $C_{14}H_9NO_2$: C 75.33, H 4.06, N 6.27; found C 77.25, H 4.01, N 6.42. Positive ESI-MS (m/z): 224 ($M - H^+$), 246 ($M - Na^+$), 262 ($M - K^+$).

Synthesis of $phendoxH_2$. To an orange suspension of 9,10-phenanthrenedione (2.08 g, 10.0 mmol) in EtOH (50 mL) was added a solution of $NH_2OH{\cdot}HCl$ (1.63 g, 25.0 mmol) and pyridine (2.03 mL, 25.0 mmol) in the same solvent (30 mL). The resulting orange suspension was refluxed for 22 h, during which time the solids dissolved and the solution turned to clear yellow. The resulting solution was cooled, filtered, and left for slow evaporation at room temperature. The next day, a yellow microcrystalline solid of the titled dioxime was formed, which was collected by fitration, washed with cold EtOH (2 × 5 mL), and dried under vacuum for 24 h. The yield was 92%. M.p.: 156−158 °C. ^1H NMR (DMSO-d_6, 400 MHz) δ (ppm): 11.91−12.69 (m, 2H), 8.70 (2H, dd, J = 1.5 Hz), 8.30 (2H, dd, J = 1.5 Hz), 7.43 (2H, dd, J = 4.5 Hz). Elemental analysis (%) calcd for $C_{14}H_{10}N_2O_2$: C 70.58, H 4.23, N 11.76; found C 70.46, H 4.13, N 11.92. Positive ESI-MS (m/z): 239 ($M - H^+$), 261 ($M - Na^+$).

Synthesis of $[Cu_3LnCl_3(phenox)_6(MeOH)_3]$ (Ln = Gd (1), Tb (2), Dy (3)). All complexes were prepared in the same manner using the corresponding lanthanide(III) chloride salts. To a stirred, orange solution of phenoxH (0.05 g, 0.20 mmol) and NEt_3 (56 μL, 0.40 mmol) in a solvent mixture comprising MeOH/MeCN (20 mL, 5:1 v/v) were added together solids $CuCl_2{\cdot}2H_2O$ (0.02 g, 0.10 mmol) and $LnCl_3{\cdot}6H_2O$ [0.07 g (Ln = Gd and Tb), 0.08 g (Ln = Dy), 0.20 mmol]. The resulting dark red solution was stirred for 40 min, during which time all solids dissolved and the solution turned to dark brown. The resulting solution was filtered, and the filtrate was left to evaporate slowly at room temperature. After 7−10 days (depending on the Ln), brown crystals of complexes **1**−**3** were formed; the crystals were collected by filtration, washed with cold MeOH (2 × 1 mL) and MeCN (2 × 2 mL), and dried in air. The yields were 40% (**1**), 46% (**2**), 30% (**3**). Anal. Calcd for the lattice solvate-free $C_{87}H_{60}N_6Cu_3GdO_{15}Cl_3$ (**1**): C, 55.47; H, 3.21; N, 4.46%. Found: C, 55.68; H, 3.47; N, 4.24%. Anal. Calcd for the lattice solvate-free $C_{87}H_{60}N_6Cu_3TbO_{15}Cl_3$ (**2**): C, 55.42; H, 3.21; N, 4.46%. Found: C, 55.55; H, 3.47; N, 4.21%. Anal. Calcd for $C_{87}H_{60}N_6Cu_3DyO_{15}Cl_3$ (**3**): C, 55.32; H, 3.20; N, 4.45%. Found: C, 55.43; H, 3.32; N, 4.36%.

DOI: 10.1021/acs.inorgchem.8b02495
Inorg. Chem. XXXX, XXX, XXX−XXX

Table 1. Crystal Data and Structural Refinement Parameters for Compounds 1 and 2

	1	2·4MeCN
empirical formula	$C_{86.25}H_{57.75}N_6O_{15}Cu_3GdCl_3$	$C_{89}H_{63}N_7O_{15}Cu_3TbCl_3$
FW/g mol^{-1}	1872.35	1926.35
temp/K	100(2)	173(1)
crystal system	triclinic	monoclinic
space group	$P\bar{1}$	$P2_1/c$
a/Å	14.1414(15)	24.0242(3)
b/Å	15.3887(17)	17.4143(2)
c/Å	22.197(2)	20.3222(2)
α/deg	98.412(3)	90
β/deg	91.374(3)	104.287(1)
γ/deg	113.192(3)	90
volume/Å^3	4374.5(8)	8239.1(2)
Z	2	4
ρ_{calc}/g cm^{-3}	1.421	1.553
μ/mm^{-1}	1.623	6.488
F(000)	1878	3876
radiation	Mo Kα (λ = 0.71073)	Cu Kα (λ = 1.54184)
index ranges	$-16 \le h \le 16$	$-28 \le h \le 27$
	$-18 \le k \le 18$	$-20 \le k \le 20$
	$-26 \le l \le 26$	$-18 \le l \le 24$
reflns collected	169848	54165
data/restraints/parameters	15414/2353/1040	14579/9/1076
goodness-of-fit on F^2	1.067	0.911
final R indexes [$I \ge 2\sigma(I)$][a,b]	R_1 = 0.0518	R_1 = 0.0434
	wR_2 = 0.1075	wR_2 = 0.0894
final R indexes [all data]	R_1 = 0.0987	R_1 = 0.0606
	wR_2 = 0.1215	wR_2 = 0.1041
$(\Delta\rho)_{max,min}$/e Å^{-3}	0.776 and −0.562	0.858 and −0.699

[a] $R_1 = \sum(||F_o| - |F_c||)/\sum|F_o|$. [b] $wR_2 = [\sum[w(F_o^2 - F_c^2)^2]/\sum[w(F_o^2)^2]]^{1/2}$, $w = 1/[\sigma^2(F_o^2) + (ap)^2 + bp]$, where $p = [\max(F_o^2, 0) + 2F_c^2]/3$.

The IR spectra and the associated bands of all complexes **1**−**3** are shown in Figure S1; the superposition of the IR bands of **1**−**3** further demonstrates their similar solid-state structures. The chemical and structural identities of **1** and **2** were also confirmed by single-crystal X-ray diffraction studies. In the case of **3**, we were not able to grow single crystals of sufficient size, and thus, the acquisition of an X-ray data set was not possible. Regardless, we have confirmed the identity of **3** by (i) IR spectroscopic comparison with the authentic, single-crystalline samples of **1** and **2**, and (ii) CHN elemental analyses.

X-ray Crystallography. A crystal of complex **1** was selected and mounted on MiteGen dual thickness micromounts using inert oil.[15] Diffraction data for **1** were collected on a D8 VENTURE diffractometer equipped with a multilayer mirror monochromator and a Mo Kα microfocus sealed tube (λ = 0.71073 Å). Images were processed with the software SAINT+,[16a,b] and absorption effects were corrected with the multiscan method implemented in SADABS.[16c] The structure was solved using the Bruker SHELXTL inside the APEX-III software package and refined using the SHELXLE and PLATON programs.[17] Single-crystal X-ray diffraction data of **2** were collected on a Rigaku Oxford Diffraction XtaLAB Synergy diffractometer equipped with a HyPix-6000HE area detector at 173 K using Cu Kα (λ = 1.54184 Å) from a PhotonJet microfocus X-ray source. The structure was solved using the charge-flipping algorithm, as implemented in the program SUPERFLIP,[18] and refined by full-matrix least-squares techniques against F_0^2 using the SHELXL program[19] through the OLEX2 interface.[20] Both structures were examined using the Addsym subroutine of PLATON[21] to ensure that no additional symmetry could be applied to the models.

The non-hydrogen atoms of both crystal structures were successfully refined using anisotropic displacement parameters, and hydrogen atoms bonded to the carbon of the ligands and those of the hydroxyl groups were placed at their idealized positions using appropriate HFIX instructions in SHELXL. All of these atoms were included in subsequent refinement cycles in riding-motion approximation with isotropic thermal displacement parameters (U_{iso}) fixed at 1.2 or 1.5 × U_{eq} of the relative atom. Substantial electron density was found on the data of compounds **1** and **2**, most likely due to additional disordered solvate molecules occupying the spaces originated by the close packing of the complexes. Our efforts to properly locate, model, and refine these residues were unsuccessful, and the investigation for the total potential solvent area using the software package PLATON confirmed clearly the existence of cavities with potential solvent accessible void volume. Consequently, the original data sets were treated with the program SQUEEZE,[22] a part of the PLATON package of crystallographic software, which calculates the contribution of the smeared electron density in the lattice voids and adds this to the calculated structure factors from the structural model when refining against the .hkl file. Unit cell parameters, structure solution, and refinement details for **1** and **2** are summarized in Table 1.

RESULTS AND DISCUSSION

Synthetic Comments. The reaction between stoichiometric amounts of 9,10-phenanthrenedione, $NH_2OH{\cdot}HCl$, and pyridine as a base in refluxing EtOH has successfully led us to an orange microcrystalline solid of the targeted mono-oxime ligand, phenoxH, in quantitative yields. In contrast, the same reaction, but in an excess of $NH_2OH{\cdot}HCl$ and pyridine, yielded a yellow microcrystalline solid in yields as high as 92%, which was characterized as the dioxime phendoxH_2 ligand. In addition to the reported data in the experimental synthetic section, the IR and ESI-MS spectra of both phenoxH and phendoxH_2 are shown in Figures S2 and S3, respectively. As expected, the amounts of $NH_2OH{\cdot}HCl$ and pyridine were found to be decisive for the clean synthesis of phenoxH

DOI: 10.1021/acs.inorgchem.8b02495
Inorg. Chem. XXXX, XXX, XXX−XXX

(orange solid) and phendoxH$_2$ (yellow solid). Furthermore, the reported refluxing times (0.5 and 22 h for phenoxH and phendoxH$_2$, respectively) were also proved important for the high-purity and high-yield syntheses of the two ligands. The targeted organic molecules can also be formed in solvent MeOH, but the yields are slightly lower than the reported ones.

The organic chelates phenoxH and phendoxH$_2$ have been previously used in homometallic 3*d*-metal chemistry by Li, Chen, and Liang, yielding antiferromagnetically coupled {Ni$_2$}, {Mn$_3$}, {Mn$_6$}, and {Mn$_8$} complexes.[23] The employment of these groups in heterometallic 3*d*/4*f*-metal cluster chemistry has not been previously documented, and therefore, we decided to investigate the general Cu^{II}/Ln^{III}/phenoxH or phendoxH$_2$ reaction systems as a means of obtaining cluster compounds with unique structural characteristics and interesting magnetic properties (high-spin molecules and/or SMMs). To this end, the general reaction between $CuCl_2{\cdot}2H_2O$, $LnCl_3{\cdot}6H_2O$, phenoxH, and NEt_3 in a 1:2:2:4 molar ratio, in a solvent mixture comprising MeCN and MeOH, afforded brown crystals of a new family of $[Cu_3LnCl_3(phenox)_6(MeOH)_3]$ clusters (Ln = Gd (**1**), Tb (**2**), Dy (**3**)) in yields of 30−46% depending on the 4*f*-metal ion. The general formation of **1**−**3** is summarized in stoichiometric eq 1.

$$3CuCl_2{\cdot}2H_2O + LnCl_3{\cdot}6H_2O + 6phenoxH + 6NEt_3 + 3MeOH \xrightarrow[MeCN]{MeOH} [Cu_3LnCl_3(phenox)_6(MeOH)_3] + 6Et_3N{\cdot}HCl + 12H_2O \quad (Ln = Gd\ (\mathbf{1}),\ Tb\ (\mathbf{2}),\ Dy\ (\mathbf{3})) \qquad (1)$$

Complexes **1**−**3** are very stable under the prevailing basic conditions, and their identities are not affected by the nature of the external base. The same products, but in lower yields, were obtained when using NMe_3, NPr_3, Me_4NOH, or other similar organic bases. In contrast, there are some important synthetic parameters which were found to affect the formation and/or crystallinity of the reported compounds. First, the Cu^{II}:Ln^{III} molar ratio has to always be 1:2. When the stoichiometric 3:1 molar ratio of Cu^{II}:Ln^{III} was adapted (as a part of our efforts to optimize the conditions for a more rational synthesis of the {Cu$_3$Ln} clusters), Cu^{II}-only products (monomers and dimers) were formed and structurally characterized.[24] It appears that the excess of Cu^{II} over the Ln^{III} ions in solution facilitates eventually the formation of relatively stable {Cu$^{II}_x$/phenox} complexes in the solid state. Second, the employment of different CuX_2 and LnX_3 starting materials (i.e., X^- = NO_3^-, ClO_4^-, $CF_3SO_3^-$, and RCO_2^-) did not lead us to any new cluster compounds; these reactions afforded dark red/brown insoluble precipitates which we were unable to crystallize and eventually determine their crystal structures. Lastly, the identity and crystallinity of **1**−**3** are strongly affected by the reaction solvent mixture of MeCN and MeOH. The same reactions in pure MeCN gave brown insoluble solids which had different IR spectra than those of the {Cu$_3$Ln} clusters. When the reactions were performed in MeOH only, brown microcrystalline materials were formed in low yields; these were identified as {Cu$_3$Ln} from IR spectroscopic studies and elemental analyses.

Unfortunately, all of our synthetic attempts to prepare Cu^{II}/Ln^{III} complexes with the dioximato ligand phendoxH$_2$ have failed to produce any crystalline material as of today. The constant formation of dark-colored (green and brown) precipitates from various different reaction systems, in the presence or absence of ancillary bridging ligands (i.e., carboxylates, azides, *β*-diketones, etc.), was attributed to the instability/decomposition of phendoxH$_2$ in the presence of hard Lewis acids (i.e., lanthanides) and presumably its metal-assisted hydrolysis into the corresponding mono-oxime (phenoxH) or diketone (9,10-phenanthrenedione).

Description of Structures. Complexes **1**−**3** are very similar to each other and differ only in the lanthanide ion present and the number of lattice solvate molecules (Figure 1 and Figure S4). Complex **2** will be described in detail as a representative example. Selected interatomic distances and angles for the structurally characterized complexes **1** and **2** are listed in Table S1 and Table 2, respectively.

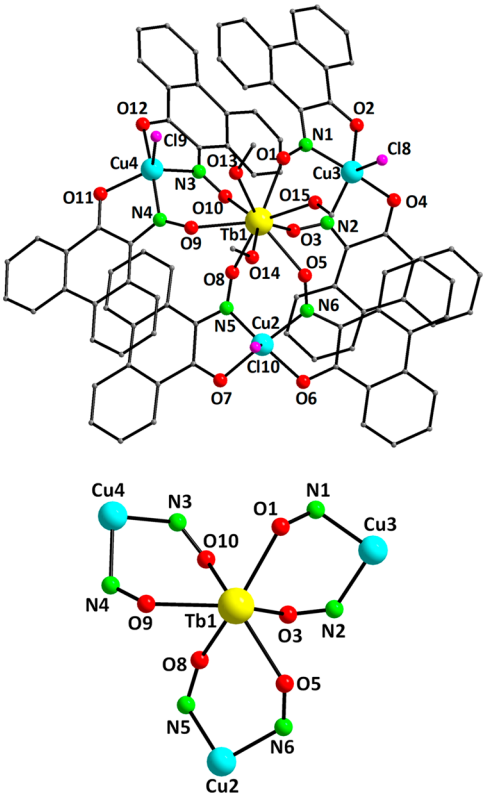

Figure 1. Labeled representation of the molecular structure of **2** (top) and its $[Cu_3Tb(\mu\text{-}NO)_6]^{3+}$ "propeller"-like core (bottom). Color scheme: Cu^{II}, cyan; Tb^{III}, yellow; Cl, purple; O, red; N, green; C, gray. H atoms are omitted for clarity.

The molecular structure of **2** (Figure 1, top) consists of a central Tb^{III} atom surrounded by three Cu^{II} atoms in a "propeller"-like conformation. Although a similar metal topology has been previously reported,[25] complexes **1**−**3** are the first oximato-bridged {Cu$_3$Ln} clusters. Six deprotonated phenox$^-$ ligands serve to bridge the Tb^{III} atom with the outer Cu^{II} atoms through their oximato groups. The carbonyl O atoms of the phenox$^-$ ligands act terminally to the Cu^{II} atoms, and together with the oximato N atoms, they form stable five-membered chelate rings. The phenox$^-$ ligands are thus bridging in an overall $\eta^1{:}\eta^1{:}\eta^1{:}\mu$ mode, contributing to the formation of the $[Cu_3Tb(\mu\text{-}NO)_6]^{3+}$ core (Figure 1, bottom). The {Cu$_3$Tb} core has a virtual D_3 symmetry. Peripheral ligation about the core is further provided by three terminally

DOI: 10.1021/acs.inorgchem.8b02495
Inorg. Chem. XXXX, XXX, XXX−XXX

Table 2. Selected Interatomic Distances (Å) and Angles (deg) for Complex 2

Tb1−O1	2.483(3)	Cu2−N6	1.971(4)
Tb1−O3	2.355(3)	Cu2−Cl10	2.326(1)
Tb1−O5	2.491(3)	Cu3−O2	2.017(3)
Tb1−O8	2.346(3)	Cu3−O4	1.999(3)
Tb1−O9	2.448(3)	Cu3−N1	1.965(4)
Tb1−O10	2.370(3)	Cu3−N2	1.998(3)
Tb1−O13	2.419(3)	Cu3−Cl8	2.366(1)
Tb1−O14	2.411(3)	Cu4−O11	2.042(3)
Tb1−O15	2.424(3)	Cu4−O12	2.005(3)
Cu2−O6	2.012(3)	Cu4−N3	1.994(4)
Cu2−O7	1.991(3)	Cu4−N4	1.967(4)
Cu2−N5	1.976(4)	Cu4−Cl9	2.327(2)
Cu2−N5−O8−Tb1	36.5(6)	Cu3−N2−O3−Tb1	48.3(5)
Cu2−N6−O5−Tb1	35.5(5)	Cu4−N3−O10−Tb1	46.3(5)
Cu3−N1−O1−Tb1	37.6(5)	Cu4−N4−O9−Tb1	48.9(5)

bound Cl^- ions, each on the Cu^{II} atoms, and three terminal MeOH molecules on the central Tb^{III} atom. The Cl^- ions are hydrogen-bonded to the MeOH groups, thus enhancing the overall stability and crystallinity of **2**. Furthermore, the three Cu^{II} atoms seem to occupy the vertices of a distorted equilateral triangle (Cu2···Cu3 = 7.090 Å, Cu3···Cu4 = 7.137 Å, and Cu2···Cu4 = 7.296 Å; Cu2−Cu4−Cu3 = 58.8°, Cu3−Cu2−Cu4 = 59.5°, and Cu4−Cu3−Cu2 = 61.7°), while the central Tb^{III} atom is displaced 1.135 Å above the Cu_3 plane. Finally, the Cu^{II} atoms are not directly linked to each other but only through the long (NO)-Ln-(NO) pathway; hence, there are no significant interactions to expect between the 3*d*-metal ions. From a supramolecular perspective, both complexes **1** and **2** exhibit some weak intermolecular $\pi-\pi$ stacking interactions between the aromatic rings of neighboring phenox$^-$ ligands (Figure S5).

All Cu^{II} atoms are five-coordinate with very distorted geometries, as confirmed by their trigonality indices, τ,[26] which gave values of 0.47, 0.57, and 0.67 for Cu2, Cu3, and Cu4, respectively (where τ is 0 and 1 for perfect square pyramidal and trigonal bipyramidal geometries, respectively). In all cases, the Cl^- ions occupy one of the apical positions. The central Tb^{III} atom, as well as the Gd^{III} atom in **1**, is nine-coordinate, surrounded by nine O atoms, and it possesses a spherical tricapped trigonal prismatic geometry. This was confirmed by the so-called continuous shape measures (CShM) approach of the SHAPE program,[27,28] which allows one to numerically evaluate by how much a particular polyhedron deviates from the ideal shape. The best fit was obtained for the spherical tricapped trigonal prism (CShM values = 0.30 for Gd^{III} and 0.36 for Tb^{III}; Figure 2 and Table S2). Values of CShM between 0.1 and 3 usually correspond to a not negligible, but still small, distortion from ideal geometry. We have recently reported a symmetric $\{Dy_2\}$ complex with the Dy^{III} atoms possessing a unique spherical tricapped trigonal prismatic geometry.[29] As a result of that unusual polyhedron, a large axiality and consequently an appreciable energy barrier for the magnetization reversal was observed.

Solid-State Magnetic Susceptibility Studies. Solid-state direct-current (*dc*) magnetic susceptibility (χ_M) data were collected on air-dried and analytically pure samples of **1**−**3** in the 2.0−300 K temperature range and are plotted as $\chi_M T$ versus T in Figure 3. The room temperature $\chi_M T$ value of complex **1** is 9.14 $cm^3 \cdot K \cdot mol^{-1}$, close to the spin-only value of

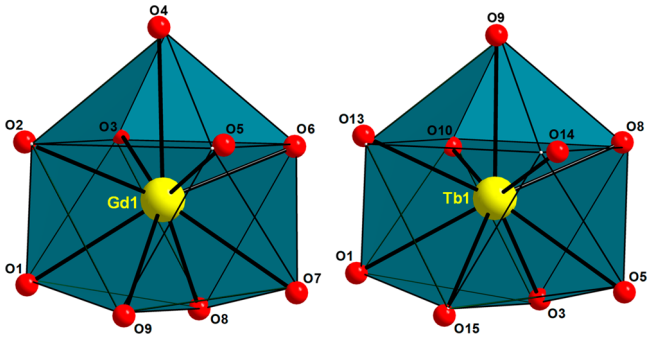

Figure 2. Spherical tricapped trigonal prismatic coordination geometries of Gd1 (left) and Tb1 (right) atoms in the structures of **1** and **2**, respectively. Points connected by the black thin lines define the vertices of the ideal polyhedron.

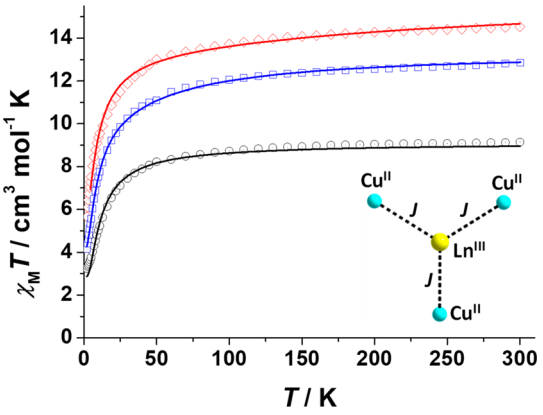

Figure 3. $\chi_M T$ versus T plots for complexes **1** (black circles), **2** (blue squares), and **3** (red diamonds). The solid lines are the fits of the data; see the text for the spin Hamiltonian and the corresponding fit parameters. (inset) *J*-coupling scheme employed for the determination of the fit parameters.

9.00 $cm^3 \cdot K \cdot mol^{-1}$ expected for one Gd^{III} ($S = 7/2$, $L = 0$) and three Cu^{II} noninteracting atoms. On cooling, the $\chi_M T$ product decreases monotonically down to a final value of 3.24 $cm^3 \cdot K \cdot mol^{-1}$ at 2 K, suggesting an overall antiferromagnetic behavior. Complexes **2** and **3** exhibit room temperature $\chi_M T$ values of 12.85 and 14.67 $cm^3 \cdot K \cdot mol^{-1}$, respectively. These are in agreement with the expected $\chi_M T$ values of three Cu^{II} and one Tb^{III} ($^7F_6$ free ion; $S = 3$; $L = 3$; $g_J = 3/2$) or Dy^{III} ($^6H_{15/2}$ free ion; $S = 5/2$; $L = 5$; $g_J = 4/3$) atoms of 12.92 and 15.30 $cm^3 \cdot K \cdot mol^{-1}$, respectively. Upon decreasing temperature, the $\chi_M T$ products continuously decrease down to 4.15 and 5.66 $cm^3 \cdot K \cdot mol^{-1}$ at 2 K.

The Cu^{II} atoms in **1**−**3** are not directly linked by any bridge, and neglecting the $Cu^{II}\cdots Cu^{II}$ interactions, the only effective superexchange pathways are those mediated by the double diatomic oximato bridges between the Cu^{II} and Ln^{III} atoms (1*J*-model, inset of Figure 3). On the basis of this simple, but effective, model, the experimental data were fit on the basis of the proposal reported by Lloret and co-workers for highly axial symmetric lanthanide environments.[30] The applied Hamiltonian is shown in eq 2, where $\hat{S}_{1\text{-}3}$ and $\hat{S}$ are the spin operators of the three Cu^{II} and Ln^{III} atoms, respectively. Furthermore, the *J* coupling constant describes the $Cu^{II}\cdots Ln^{III}$ interactions, λ is the spin−orbit coupling parameter, Δ parametrizes the axial zero-field splitting of the Ln^{III} atom, and κ is an orbital reduction parameter. The first term of the Hamiltonian gives

DOI: 10.1021/acs.inorgchem.8b02495
Inorg. Chem. XXXX, XXX, XXX−XXX

the interaction between the spin of the Cu^{II} atoms and the spin component of the Ln^{III}. The second term describes the spin−orbit coupling, the third term accounts for an axial ligand-field component around the Ln^{III} atoms, and the last term is the Zeeman effect.[30]

$$\hat{H} = -2J(\hat{S}_1\cdot\hat{S} + \hat{S}_2\cdot\hat{S} + \hat{S}_3\cdot\hat{S}) + \lambda\hat{L}\hat{S} + \Delta[\hat{L}_z^{\,2} - L(L+1)/3] + \beta H(-\kappa\hat{L} + 2\hat{S}) \quad (2)$$

In the case of $\{Cu_3Gd\}$ (**1**), the above Hamiltonian reduces to the conventional isotropic spin Hamiltonian of eq 3.

$$\hat{H} = -2J(\hat{S}_1\cdot\hat{S} + \hat{S}_2\cdot\hat{S} + \hat{S}_3\cdot\hat{S}) \quad (3)$$

A very good fit of the experimental data for **1** using eq 3 was obtained (solid line in Figure 3), and the corresponding best-fit parameters were $J = -1.34$ cm^{-1} and $g = 2.10$ ($R = 6.3 \times 10^{-4}$). The resulting antiferromagnetic interactions between the Cu^{III} and Gd^{III} atoms lead to a rational (using the "spin-up"/"spin-down" vector scheme) ground state spin value of $S = 2$. This is also in excellent agreement with the recorded magnetization data of **1** at 2 K (Figure 4), which show a regular increase that

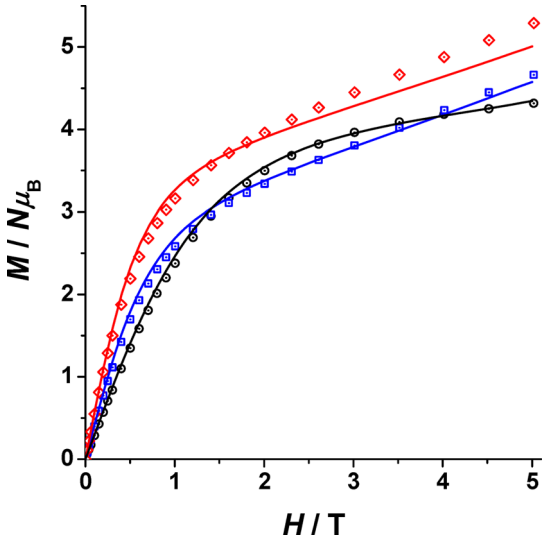

Figure 4. Magnetization (M) versus field (H) plots for complexes **1** (black circles), **2** (blue squares), and **3** (red diamonds). Solid lines show the simulation of M with the values obtained from the magnetic susceptibility fits.

tends to a value of 4.32 $N\mu_B$ under the maximum applied field of 5 T. For the anisotropic complexes **2** and **3**, the experimental data were perfectly fit to the Hamiltonian of eq 2. The best-fit parameters were $J = -1.42$ cm^{-1}, $g_{Cu} = 2.10$, and $\Delta = -26.3$ cm^{-1} ($R = 4.0 \times 10^{-5}$) for **2**, and $J = -1.70$ cm^{-1}, $g_{Cu} = 2.05$, and $\Delta = -38.1$ cm^{-1} ($R = 4.0 \times 10^{-5}$) for **3**. The relatively small value of g_{Cu} for **3** is due to the fixed orbital reduction parameter, κ, in the fitting Hamiltonian. The κ parameter could range between 0.95 and 1 as a function of the covalency. To avoid overparametrization, we have fixed the value of κ as 1. A lower κ value will be compensated with a larger g_{Cu}. Indeed, an alternative good fitting of the experimental data of **3** with $\kappa = 0.985$ gives the following best-fit parameters: $J = -1.60$ cm^{-1}, $g_{Cu} = 2.10$, and $\Delta = -33.0$ cm^{-1}. The negative sign of Δ suggests that the superexchange interactions take place between the three $S_{Cu} = 1/2$ and the lanthanide's $M_J = 6$ (for Tb) or 15/2 (for Dy) levels.[30] The obtained J values and subsequently the antiferromagnetic behavior of **1**−**3** agree well with previously reported oximato-bridged Cu/Ln complexes.[31] This is rationalized in terms of the degree of distortion of the {Cu-N-O-Ln} magnetic exchange pathways. For planar {Cu-N-O-Gd} units, the interactions are expected to be ferromagnetic, but for large Cu−N−O−Gd torsion angles, such as those of complexes **1**−**3**, the coupling switches to antiferromagnetic.[32]

The magnetization (M) versus field (H) plots of **2** and **3** show a similar characteristic shape, with a fast increase of M in the 0−1 T field range and a constant increase of M in larger fields to reach a nonsaturated value of 4.66 and 5.29 $N\mu_B$ at the maximum applied field of 5 T (Figure 4). It is remarkable that the magnetization plots of **2** and **3** can be reproduced in values and shapes with the J and Δ parameters obtained by the magnetic susceptibility fits. It is important to mention at this point that this fitting procedure, implemented in the program PHI, is here used for the first time. Even if this method is only valid in highly symmetric environments, when it is properly used, it allows a very simple and efficient method to elucidate the exchange parameters, avoiding more detailed, but complicated, methods. However, the reported procedure can be only used in very specific and selected examples. It is also worthy to mention that all previously reported $\{Cu_3Ln\}$ complexes with a "propeller"-like metal topology have the same $[Cu_3Ln(\mu\text{-}OR)_6]^{3+}$ cores,[25] where R belongs to the scaffold of different macrocyclic and alkoxide-based chelates. In all of these alkoxido-bridged $\{Cu_3Ln\}$ complexes, the metal ions are ferromagnetically coupled and the compounds exhibit SMM properties depending on the Ln^{III}.[25] In addition, Tang, Clérac, and co-workers have reported $\{M^{III}Dy_3\}$ (M^{III} = Fe and Co) complexes with a three-blade "propeller" conformation, where the 3d-metal ions occupy the central position and they are bridged to the external Dy^{III} ions through three dithiooxalato ligands.[33] The long magnetic pathways induced very weak intramolecular magnetic interactions between the spin carriers, while both compounds exhibited SMM properties with fast relaxation of their magnetization.

In light of the negative anisotropy of compounds **2** and **3**, alternating current (ac) magnetic susceptibility studies were performed in the 1.8−7.0 K range using a 4.0 Oe ac field oscillating at frequencies in the 10−1500 Hz range. The ac measurements at zero external dc field revealed very weak tails of out-of-phase (χ''_M) signals for both **2** and **3**, which were enhanced under a transverse field of 1000 G, indicating the presence of quantum tunneling of magnetization. Thus, the ac measurements as a function of temperature and frequency were performed under an external dc field of 1000 G. The χ''_M versus T plots for **2** and **3** are presented in Figure 5, and they both show the absence of resolved peak maxima due to the blocking of the magnetization. However, **2** and **3** show well-defined frequency-dependent tails of peaks below ∼5 K, which are indicative of the slow relaxation of magnetization of an SMM.

Assuming that the relaxation process has only one characteristic time corresponding to a Debye relaxation process, the SMM parameters can be elucidated through the Arrhenius law: $\tau(T) = \exp(E_a/k_BT)$. By using the Kramers−Kronig equations,[34] which combine the real and imaginary parts of a function and relate χ'' with χ_T and χ_S, where χ_T and χ_S are the isothermal and adiabatic susceptibilities, respectively, the eq 4 can be derived.

DOI: 10.1021/acs.inorgchem.8b02495
Inorg. Chem. XXXX, XXX, XXX−XXX

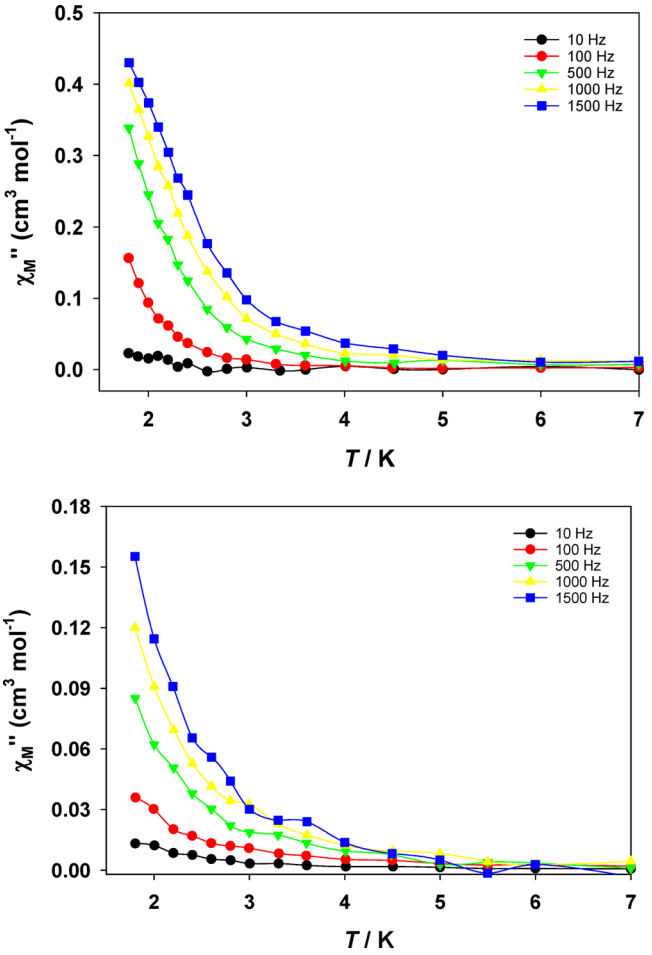

Figure 5. Temperature dependence of the out-of-phase (χ_M'') *ac* magnetic susceptibility under an applied *dc* field of 1000 G for complexes **2** (top) and **3** (bottom) at the indicated frequencies. Solid lines are guides for the eye only.

$$\ln(\chi''/\chi') = \ln(\omega\tau_0) + U_{eff}/k_BT \quad (4)$$

In eq 4, ω is the angular frequency, τ_0 is the pre-exponential factor, which provides a quantitative measure of the attempt time of relaxation from the thermal phonon bath and its value is usually within the 10^{-6}–10^{-10} s range, U_{eff} is the effective energy barrier for the magnetization reversal, and k_B is the Boltzmann's constant. Equation 4 is a valuable tool in the absence of out-of-phase peak maxima from the χ''_M versus T plots and allows one to determine the important SMM parameters, U_{eff} and τ_0. On the basis of eq 4, the best-fit parameters obtained for complexes **2** and **3** (Figure 6) were U_{eff} = 10.1 cm^{-1} and $\tau_0 = 1.7 \times 10^{-6}$ s, and U_{eff} = 5.4 cm^{-1} and $\tau_0 = 5.1 \times 10^{-6}$ s, respectively. The resulting energy barriers are small and much lower than the energy gap between the ground and the first excited states, and thus an Orbach process must be excluded as an efficient magnetization relaxation process for complexes **2** and **3**.[35]

CONCLUSIONS

In conclusion, we have reported an unprecedented family of {Cu_3Ln} complexes with a "propeller"-like topology, in which the outer Cu^{II} and central Ln^{III} atoms are exclusively bridged by the diatomic oximato groups of six deprotonated phenoxH (9,10-phenanthrenedione-9-oxime) ligands. Due to the large

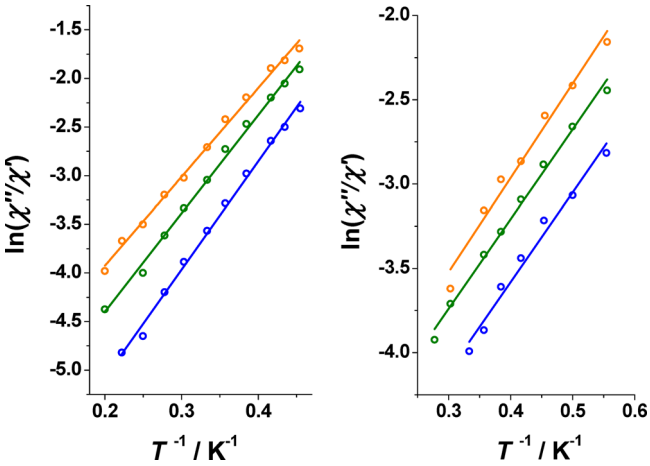

Figure 6. Debye plots of complexes **2** (left) and **3** (right) for the frequencies 1500 (orange), 1000 (green), and 500 (blue) Hz. The solid lines correspond to the fit of the data by applying eq 4; see the text for the fit parameters.

distortions of the {Cu-N-O-Ln} bridging units, the reported compounds exhibit antiferromagnetic exchange interactions. However, the presence of magnetic anisotropy has contributed to the onset of slow magnetization relaxation for the {Cu_3Tb} and {Cu_3Dy} analogues, albeit with small energy barriers of 10.1 and 5.4 cm^{-1}, respectively. A new fitting method, implemented in the program PHI, is here used for the first time and allowed for the determination of the magnetic exchange parameters in highly symmetric lanthanide environments. A very good fit of the magnetic susceptibility data gave the parameters: J = −1.34 cm^{-1} and g = 2.10 (for **1**), J = −1.42 cm^{-1}, g_{Cu} = 2.10, and Δ = −26.3 cm^{-1} (for **2**), and J = −1.70 cm^{-1}, g_{Cu} = 2.05, and Δ = −38.1 cm^{-1} (for **3**), thus confirming the antiferromagnetic interactions between the Cu^{II} and Ln^{III} atoms and the presence of negative magnetic anisotropy. Our synthetic efforts are currently oriented toward the accomplishment of two short-term research objectives: (i) the deliberate replacement of the outer Cu^{II} atoms by other divalent 3*d*-metal ions (i.e., Ni^{II} and Zn^{II}) without disturbing the "propeller"-like core, and (ii) the chemical manipulation of the lanthanides' polyhedra by removing the coordinated MeOH molecules and/or substituting them with anionic groups.

ASSOCIATED CONTENT

Supporting Information

The Supporting Information is available free of charge on the ACS Publications website at DOI: 10.1021/acs.inorgchem.8b02495.

Various structural and spectroscopic figures (PDF)

Accession Codes

CCDC 1864722 and 1864723 contain the supplementary crystallographic data for this paper. These data can be obtained free of charge via www.ccdc.cam.ac.uk/data_request/cif, or by emailing data_request@ccdc.cam.ac.uk, or by contacting The Cambridge Crystallographic Data Centre, 12 Union Road, Cambridge CB2 1EZ, UK; fax: +44 1223 336033.

AUTHOR INFORMATION

Corresponding Author

*E-mail: tstamatatos@brocku.ca.

DOI: 10.1021/acs.inorgchem.8b02495
Inorg. Chem. XXXX, XXX, XXX−XXX

ORCID

Di Sun: 0000-0001-5966-1207
Christos Lampropoulos: 0000-0001-9065-1453
Theocharis C. Stamatatos: 0000-0002-9798-9331

Notes

The authors declare no competing financial interest.

■ ACKNOWLEDGMENTS

This work was supported by NSERC-DG, ERA, Brock University (Chancellor's Chair for Research Excellence) to Th.C.S. C.L. acknowledges support from the National Science Foundation (NSF 1429428 and 1626332) and the CCSA Research Corporation for Science Advancement. A.E and J.M thank the Ministerio de Economia y Competitividad (Project CTQ2015-63614-P) for the financial support. This work was also funded by the National Natural Science Foundation of China (Grant Nos. 21822107 and 21571115).

■ REFERENCES

(1) For high-nuclearity Cu^{II}/Ln^{III} clusters, see: (a) Leng, J.-D.; Liu, J.-L.; Tong, M.-L. Unique nanoscale $\{Cu^{II}_{36}Ln^{III}_{24}\}$ (Ln = Dy and Gd) metallo-rings. *Chem. Commun.* **2012**, *48*, 5286−5288. (b) Dermitzaki, D.; Lorusso, G.; Raptopoulou, C. P.; Psycharis, V.; Escuer, A.; Evangelisti, M.; Perlepes, S. P.; Stamatatos, Th. C. Molecular Nanoscale Magnetic Refrigerants: A Ferrimagnetic $\{Cu^{II}_{15}Gd^{III}_{7}\}$ Cagelike Cluster from the Use of Pyridine-2,6-dimethanol. *Inorg. Chem.* **2013**, *52*, 10235−10237. (c) Xiong, G.; Xu, H.; Cui, J. Z.; Wang, Q. L.; Zhao, B. The multiple core−shell structure in $Cu_{24}Ln_6$ cluster with magnetocaloric effect and slow magnetization relaxation. *Dalton Trans.* **2014**, *43*, 5639−5642. (d) Xiang, S.; Hu, S.; Sheng, T.; Fu, R.; Wu, X.; Zhang, X. A. A Fan-Shaped Polynuclear Gd_6Cu_{12} Amino Acid Cluster: A "Hollow" and Ferromagnetic $[Gd_6(\mu_3\text{-}OH)_8]$ Octahedral Core Encapsulated by Six $[Cu_2]$ Glycinato Blade Fragments. *J. Am. Chem. Soc.* **2007**, *129*, 15144−15146. (e) Zhang, J.- J.; Hu, S.- M.; Xiang, S.- C.; Sheng, T.; Wu, X.-T.; Li, Y.-M. Syntheses, Structures, and Properties of High-Nuclear 3d−4f Clusters with Amino Acid as Ligand: $\{Gd_6Cu_{24}\}$, $\{Tb_6Cu_{26}\}$, and $\{(Ln_6Cu_{24})_2Cu\}$ (Ln= Sm, Gd). *Inorg. Chem.* **2006**, *45*, 7173−7181. (f) Wu, J.; Zhao, L.; Zhang, L.; Li, X.-L.; Guo, M.; Powell, A. K.; Tang, J. Macroscopic Hexagonal Tubes of 3d-4f Metallocycles. *Angew. Chem., Int. Ed.* **2016**, *55*, 15574−15578. (g) Wu, J.; Zhao, L.; Zhang, L.; Li, X.- L.; Guo, M.; Tang, J. Metallosupramolecular Coordination Complexes: The Design of Heterometallic 3d−4f Gridlike Structures. *Inorg. Chem.* **2016**, *55*, 5514−5519. (h) Baskar, V.; Gopal, K.; Helliwell, M.; Tuna, F.; Wernsdorfer, W.; Winpenny, R. E. P. 3d−4f Clusters with Large Spin Ground States and SMM Behaviour. *Dalton Trans.* **2010**, *39*, 4747−4750.

(2) Andruh, M.; Ramade, I.; Codjovi, E.; Guillou, O.; Kahn, O.; Trombe, J.-C. Crystal structure and magnetic properties of $[Ln_2Cu_4]$ hexanuclear clusters (where Ln = trivalent lanthanide). Mechanism of the gadolinium(III)-copper(II) magnetic interaction. *J. Am. Chem. Soc.* **1993**, *115*, 1822−1829.

(3) (a) Costes, J.-P.; Duhayon, C.; Mallet-Ladeira, S.; Vendier, L.; Garcia-Tojal, J.; Lopez Banet, L. Antiferromagnetic Cu−Gd interactions through an oxime bridge. *Dalton Trans.* **2014**, *43*, 11388−11396. (b) Cremades, E.; Gomez-Coca, S.; Aravena, D.; Alvarez, S.; Ruiz, E. Theoretical Study of Exchange Coupling in 3d-Gd Complexes: Large Magnetocaloric Effect Systems. *J. Am. Chem. Soc.* **2012**, *134*, 10532−10542. (c) Ramade, I.; Kahn, O.; Jeannin, Y.; Robert, F. Design and Magnetic Properties of a Magnetically Isolated $Gd^{III}Cu^{II}$ Pair. Crystal Structures of $[Gd(hfa)_3Cu(salen)]$, $[Y(hfa)_3Cu(salen)]$, $[Gd(hfa)_3Cu(salen)(Meim)]$, and $[La(hfa)_3(H_2O)Cu(salen)]$ [hfa = Hexafluoroacetylacetonato, salen = N,N′-Ethylenebis(salicylideneaminato), Meim = 1-Methylimidazole]. *Inorg. Chem.* **1997**, *36*, 930−936. (d) Koner, R.; Lin, H.-H.; Wei, H.-H.; Mohanta, S. Syntheses, Structures, and Magnetic Properties of Diphenoxo-Bridged $M^{II}Ln^{III}$ Complexes Derived from *N,N′*-Ethylenebis(3-ethoxysalicylaldiimine) (M = Cu or Ni; Ln = Ce-Yb): Observation of Surprisingly Strong Exchange Interactions. *Inorg. Chem.* **2005**, *44*, 3524−3536.

(4) (a) Evangelisti, M. In *Molecular Magnets: Physics and Applications*; Bartolomé, J., Luis, F., Fernández, J. F., Eds.; Springer: Berlin, 2014; pp 365−387. (b) Evangelisti, M.; Luis, F.; de Jongh, L. J.; Affronte, M. J. Magnetothermal properties of molecule-based materials. *J. Mater. Chem.* **2006**, *16*, 2534−2549.

(5) For example, see: (a) Evangelisti, M.; Brechin, E. K. Recipes for enhanced molecular cooling. *Dalton Trans.* **2010**, *39*, 4672−4676. (b) Evangelisti, M.; Roubeau, O.; Palacios, E.; Camón, A.; Hooper, T. N.; Brechin, E. K.; Alonso, J. J. Cryogenic Magnetocaloric Effect in a Ferromagnetic Molecular Dimer. *Angew. Chem., Int. Ed.* **2011**, *50*, 6606−6609. (c) Langley, S. K.; Chilton, N. F.; Moubaraki, B.; Hooper, T.; Brechin, E. K.; Evangelisti, M.; Murray, K. S. Molecular coolers: The case for $[Cu^{II}_5Gd^{III}_4]$. *Chem. Sci.* **2011**, *2*, 1166−1169.

(6) (a) Gatteschi, D.; Sessoli, R.; Villain, J. *Molecular Nanomagnets*; Oxford University Press: Oxford, U.K., 2006. (b) Rinehart, J. D.; Long, J. R. Exploiting single-ion anisotropy in the design of f-element single-molecule magnets. *Chem. Sci.* **2011**, *2*, 2078−2085. (c) Layfield, R.; Murugesu, M. *Lanthanides and Actinides in Molecular Magnetism*; Wiley-VCH: Weinheim, Germany, 2015.

(7) For example, see: (a) Feltham, H. L. C.; Brooker, S. Review of purely 4f and mixed-metal nd-4f single-molecule magnets containing only one lanthanide ion. *Coord. Chem. Rev.* **2014**, *276*, 1−33 (Review) . (b) Murrie, M. Bis-tris propane as a flexible ligand for high-nuclearity complexes. *Polyhedron* **2018**, *150*, 1−9 (Review) . (c) Alexandropoulos, D. I.; Cunha-Silva, L.; Tang, J.; Stamatatos, Th. C. Heterometallic Cu/Ln cluster chemistry: ferromagnetically-coupled $\{Cu_4Ln_2\}$ complexes exhibiting single-molecule magnetism and magnetocaloric properties. *Dalton Trans.* **2018**, *47*, 11934−11941. (d) Alexandropoulos, D. I.; Cunha-Silva, L.; Lorusso, G.; Evangelisti, M.; Tang, J.; Stamatatos, Th. C. Dodecanuclear 3d/4f-metal clusters with a 'Star of David' topology: single-molecule magnetism and magnetocaloric properties. *Chem. Commun.* **2016**, *52*, 1693−1696.

(8) (a) Alaimo, A. A.; Worrell, A.; Das Gupta, S.; Abboud, K. A.; Lampropoulos, C.; Christou, G.; Stamatatos, Th. C. Structural and Magnetic Variations in a Family of Isoskeletal, Oximate-Bridged $\{Mn^{IV}_2M^{III}\}$ Complexes (M^{III}=Mn, Gd, Dy). *Chem. - Eur. J.* **2018**, *24*, 2588−2592. (b) Alexandropoulos, D. I.; Manos, M. J.; Papatriantafyllopoulou, C.; Mukherjee, S.; Tasiopoulos, A. J.; Perlepes, S. P.; Christou, G.; Stamatatos, Th. C. Squaring the clusters": a $Mn^{III}_4Ni^{II}_4$ molecular square from nickel(II)-induced structural transformation of a $Mn^{II/III/IV}_{12}$ cage. *Dalton Trans.* **2012**, *41*, 4744−4747. (c) Papatriantafyllopoulou, C.; Stamatatos, Th. C.; Efthymiou, C. G.; Cunha-Silva, L.; Almeida Paz, F. A.; Perlepes, S. P.; Christou, G. A High-Nuclearity 3d/4f Metal Oxime Cluster: An Unusual Ni_8Dy_8 "Core-Shell" Complex from the Use of 2-Pyridinealdoxime. *Inorg. Chem.* **2010**, *49*, 9743−9745.

(9) Alexandropoulos, D. I.; Poole, K. M.; Cunha-Silva, L.; Ahmad Sheikh, J.; Wernsdorfer, W.; Christou, G.; Stamatatos, Th. C. A family of 'windmill'-like $\{Cu_6Ln_{12}\}$ complexes exhibiting single-molecule magnetism behavior and large magnetic entropy changes. *Chem. Commun.* **2017**, *53*, 4266−4269.

(10) Richardson, P.; Gagnon, K. J.; Teat, S. J.; Lorusso, G.; Evangelisti, M.; Tang, J.; Stamatatos, T. C. New Dioximes as Bridging Ligands in 3d/4f-Metal Cluster Chemistry: One-Dimensional Chains of Ferromagnetically Coupled $\{Cu_6Ln_2\}$ Clusters Bearing Acenaphthenequinone Dioxime and Exhibiting Magnetocaloric Properties. *Cryst. Growth Des.* **2017**, *17*, 2486−2497.

(11) Katritzky, A. R.; Wang, Z.; Hall, C. D.; Akhmedov, N. G.; Shestopalov, A. A.; Steel, P. J. Cyclization of alpha-Oxo-oximes to 2-substituted benzoxazoles. *J. Org. Chem.* **2003**, *68*, 9093−9099.

(12) Putala, M.; Kastner-Pustet, N.; Mannschreck, A. Diastereoselective reaction of (MP)-pentahelicene-7,8-dione with trans-cyclohexane-1,2-diamine. Thermal and photochemical transformations of its product. *Tetrahedron: Asymmetry* **2002**, *12*, 3333−3342.

DOI: 10.1021/acs.inorgchem.8b02495
Inorg. Chem. XXXX, XXX, XXX−XXX

(13) Chilton, N. F.; Anderson, R. P.; Turner, L. D.; Soncini, A.; Murray, K. S. PHI: a powerful new program for the analysis of anisotropic monomeric and exchange-coupled polynuclear d- and f-block complexes. *J. Comput. Chem.* **2013**, *34*, 1164−1175.
(14) Bain, G. A.; Berry, J. F. Diamagnetic Corrections and Pascal's Constants. *J. Chem. Educ.* **2008**, *85*, 532−536.
(15) https://www.mitegen.com/product/loops/.
(16) (a) *SAINT+, Data Integration Engine*, version 7.23a; Bruker AXS: Madison, WI, 1997−2005. (b) *APEX2: Data Collection Software*, version 2.1-RC13; Bruker AXS Inc.: Delft, The Netherlands, 2006. (c) Sheldrick, G. M. *SADABS: Bruker/Siemens Area Detector Absorption Correction Program*, v.2.01; Bruker AXS Inc.: Madison, WI, 1998.
(17) (a) *APEX-III: Data Collection Software*; Bruker AXS Inc.: Madison, WI, 2016. (b) Hübschle, C. B.; Sheldrick, G. M.; Dittrich, B. ShelXle a Qt graphical user interface for SHELXL. *J. Appl. Crystallogr.* **2011**, *44*, 1281−1284.
(18) Palatinus, L.; Chapuis, G. SUPERFLIP − a computer program for the solution of crystal structures by charge flipping in arbitrary dimensions. *J. Appl. Crystallogr.* **2007**, *40*, 786−790.
(19) Sheldrick, G. M. Crystal structure refinement with SHELXL. *Acta Crystallogr., Sect. C: Struct. Chem.* **2015**, *71*, 3−8.
(20) Dolomanov, O. V.; Bourhis, L. J.; Gildea, R. J.; Howard, J. A. K.; Puschmann, H. OLEX2 a complete structure solution, refinement and analysis program. *J. Appl. Crystallogr.* **2009**, *42*, 339−341.
(21) Spek, A. L. Structure validation in chemical crystallography. *Acta Crystallogr., Sect. D: Biol. Crystallogr.* **2009**, *65*, 148−155.
(22) Spek, A. L. Single-crystal structure validation with the program PLATON. *J. Appl. Crystallogr.* **2003**, *36*, 7−13.
(23) (a) Chen, Z.; Hu, Z.; Li, Y.; Liang, Y.; Wang, X.; Ouyang, L.; Zhao, Q.; Cheng, H.; Liang. Manganese clusters of aromatic oximes: synthesis, structure and magnetic properties. *Dalton Trans.* **2016**, *45*, 15634−15643. (b) Li, X.; Li, B.; Hu, Z.; Cheng, H.; Zhao, Q.; Chen, Z. Structural and magnetic properties of manganese and nickel clusters with 9,10-phenanthrenedione-9-oxime ligands. *Transition Met. Chem.* **2017**, *42*, 421−426.
(24) These results are not related to the present work and they will be reported in an upcoming paper.
(25) For $[Cu_3Ln(\mu\text{-}OR)_6]^{3+}$ complexes with a "propeller"-like topology, see: (a) Benelli, C.; Blake, A. J.; Milne, P. E. Y.; Rawson, J. M.; Winpenny, R. E. P. Magnetic and Structural Studies of Copper−Lanthanoid Complexes; the Synthesis and Structures of New Cu_3Ln Complexes of 6-chloro-2-Pyridone (Ln = Gd, Dy and Er) and Magnetic Studies on Cu_2Gd_2, Cu_4Gd_2 and Cu_3Gd Complexes. *Chem. - Eur. J.* **1995**, *1*, 614−618. (b) Dhers, S.; Feltham, H. L. C.; Rouzières, M.; Clérac, R.; Brooker, S. Macrocyclic {3d−4f} SMMs as building blocks for 1D-polymers: selective bridging of 4f ions by use of an O-donor ligand. *Dalton Trans.* **2016**, *45*, 18089−18093. (c) Feltham, H. L. C.; Clérac, R.; Powell, A. K.; Brooker, S. A Tetranuclear, Macrocyclic 3d−4f Complex Showing Single-Molecule Magnet Behavior. *Inorg. Chem.* **2011**, *50*, 4232−4234. (d) Feltham, H. L. C.; Clérac, R.; Ungur, L.; Vieru, V.; Chibotaru, L. F.; Powell, A. K.; Brooker, S. Synthesis and Magnetic Properties of a New Family of Macrocyclic $M^{II}_3Ln^{III}$ Complexes: Insights into the Effect of Subtle Chemical Modification on Single-Molecule Magnet Behavior. *Inorg. Chem.* **2012**, *51*, 10603−10612. (e) Feltham, H. L. C.; Clérac, R.; Ungur, L.; Chibotaru, L. F.; Powell, A. K.; Brooker, S. By Design: A Macrocyclic 3d−4f Single-Molecule Magnet with Quantifiable Zero-Field Slow Relaxation of Magnetization. *Inorg. Chem.* **2013**, *52*, 3236−3240. (f) Kettles, F. J.; Milway, V. A.; Tuna, F.; Valiente, R.; Thomas, L. H.; Wernsdorfer, W.; Ochsenbein, S. T.; Murrie, M. Exchange Interactions at the Origin of Slow Relaxation of the Magnetization in $\{TbCu_3\}$ and $\{DyCu_3\}$ Single-Molecule Magnets. *Inorg. Chem.* **2014**, *53*, 8970−8978.
(26) Addison, A. W.; Rao, T. N.; Reedijk, J.; van Rijn, J.; Verschoor, G. C. Synthesis, structure, and spectroscopic properties of copper(II) compounds containing nitrogen−sulphur donor ligands; the crystal and molecular structure of aqua[1,7-bis(N-methylbenzimidazol-2′-yl)-2,6-dithiaheptane]copper(II) perchlorate. *J. Chem. Soc., Dalton Trans.* **1984**, *0*, 1349−1356.
(27) Alvarez, S.; Alemany, P.; Casanova, D.; Cirera, J.; Llunell, M.; Avnir, D. Shape Maps and Polyhedral Interconversion Paths in Transition Metal Chemistry. *Coord. Chem. Rev.* **2005**, *249*, 1693−1708.
(28) Zabrodsky, H.; Peleg, S.; Avnir, D. Continuous symmetry measures. *J. Am. Chem. Soc.* **1992**, *114*, 7843−7851.
(29) Mazarakioti, E. C.; Regier, J.; Cunha-Silva, L.; Wernsdorfer, W.; Pilkington, M.; Tang, J.; Stamatatos, Th. C. Large Energy Barrier and Magnetization Hysteresis at 5 K for a Symmetric $\{Dy_2\}$ Complex with Spherical Tricapped Trigonal Prismatic Dy^{III} Ions. *Inorg. Chem.* **2017**, *56*, 3568−3578.
(30) Marinho, M. V.; Reis, D. O.; Oliveira, W. X. C.; Marques, L. F.; Stumpf, H. O.; Déniz, M.; Pasán, J.; Ruiz-Pérez, C.; Cano, J.; Lloret, F.; Julve, M. Photoluminescent and Slow Magnetic Relaxation Studies on Lanthanide(III)-2,5-pyrazinedicarboxylate Frameworks. *Inorg. Chem.* **2017**, *56*, 2108−2123.
(31) Costes, J.- P.; Dahan, F.; Dupuis, A. Is Ferromagnetism an Intrinsic Property of the Cu^{II}/Gd^{III} Couple? 2. Structures and Magnetic Properties of Novel Trinuclear Complexes with μ-Phenolato-μ-oximato (Cu−Ln−Cu) Cores (Ln = La, Ce, Gd). *Inorg. Chem.* **2000**, *39*, 5994−6000.
(32) Costes, J.- P.; Vendier, L. Cu-Ln complexes with a single μ-oximato bridge. *C. R. Chim.* **2010**, *13*, 661−667.
(33) Xu, G.- F.; Gamez, P.; Tang, J.; Clérac, R.; Guo, Y.- N.; Guo, Y. $M^{III}Dy^{III}_3$ (M = Fe^{III}, Co^{III}) Complexes: Three-Blade Propellers Exhibiting Slow Relaxation of Magnetization. *Inorg. Chem.* **2012**, *51*, 5693−5698.
(34) (a) Cole, K. S.; Cole, R. H. Dispersion and Absorption in Dielectrics I. Alternating Current Characteristics. *J. Chem. Phys.* **1941**, *9*, 341−351. (b) Grahl, M.; Kotzler, J.; Sessler, I. Correlation between domain-wall dynamics and spin-spin relaxation in uniaxial ferromagnets. *J. Magn. Magn. Mater.* **1990**, *90*−*91*, 187−188. (c) Bartolomé, J.; Filoti, G.; Kuncser, V.; Schinteie, G.; Mereacre, V.; Anson, C. E.; Powell, A. K.; Prodius, D.; Turta, C. Magnetostructural correlations in the tetranuclear series of $\{Fe_3LnO_2\}$ butterfly core clusters: Magnetic and Mössbauer spectroscopic study. *Phys. Rev. B: Condens. Matter Mater. Phys.* **2009**, *80*, 014430−014446.
(35) Tang, J.; Zhang, P. *Lanthanide Single Molecule Magnets*; Springer-Verlag: Heidelberg, Germany, 2015.

DOI: 10.1021/acs.inorgchem.8b02495
Inorg. Chem. XXXX, XXX, XXX−XXX